Quantifying Plasticization and Melting Behavior of Poly(vinylidene fluoride) in Supercritical CO_2 Utilizing a Linear Variable Differential Transformer

Suresh L. Shenoy, Tomoko Fujiwara, and Kenneth J. Wynne*

Department of Chemical Engineering, Virginia Commonwealth University, 601 West Main St., Richmond, Virginia 23284-3028

Received December 6, 2002; Revised Manuscript Received March 11, 2003

ABSTRACT: Supercritical CO_2 plasticization of semicrystalline poly(vinylidene fluoride) (PVDF) was investigated by measuring linear dilation as a function of temperature (75−130 °C) and pressure (138−670 bar) using a linear variable differential transformer (LVDT). The robustness of the LVDT technique allows the study of CO_2 plasticization at high temperatures (to T_m) and pressures. Experiments at constant temperature (varying pressure) and constant pressure (varying temperature) were performed. With constant temperature experiments below 100 °C, dilation increased up to 414 bar, while at higher pressures, the change of dilation with pressure attenuated. At higher temperatures (≥117 °C), dilation increased almost linearly with pressure through the experimental range. Constant pressure experiments were carried out to assess the effect of CO_2 pressure on T_m. With increasing pressure, T_m decreased to a minimum of 135 °C at 483 bar ($\Delta T_m = 23$ °C). Above 483 bar, hydrostatic effects override plasticization and T_m increases. By comparing T_m under N_2, a gas with minimal interaction with the polymer, competition between plasticization and hydrostatic pressure on T_m is clarified.

Introduction

Supercritical carbon dioxide has been extensively investigated in polymer technologies for replacement of environmentally harmful organic solvents. A key advantage of CO_2 is the ability to manipulate solvent density as a function of temperature and pressure.[1,2] Supercritical CO_2 has been employed as a solvent for polymer synthesis,[3−5] for spin casting polymer thin films,[6] and for extraction of low molecular weight species from polymers.[1,4]

In polymer melt applications, CO_2 has been used as a blowing agent for the production of foams,[7−13] as a processing aid to reduce polymer melt viscosity [14−17] and in facilitating fiber spinning.[18] In the solid state, supercritical CO_2 plasticization has been employed to enhance the solubility of styrene in poly(tetrafluoroethylene-*co*-hexafluoropropene) followed by in situ polymerization of styrene to thereby produce polymer−polymer composites.[19] Compressed CO_2 was found to facilitate the crystallization of methyl-substituted poly(aryl ether ether ketone) and *tert*-butyl-substituted poly(ether ether ketone) (tBuPEEK), which normally do not undergo crystallization upon annealing.[20,21]

Related to these applications are investigations of CO_2 polymer plasticization, with most studies focusing on amorphous polymers.[22−28] Plasticization by high-pressure CO_2 has been investigated through sorption isotherms,[25,29,30] by measuring polymer dilation,[23,25,27,31] and by depression of glass transition temperatures (T_g).[24,26,32,33] It has been well documented that an increase in CO_2 pressure results in enhanced plasticization and reduced T_g's.[23,25,27,28]

Effects of compressed CO_2 on semicrystalline polymers have also been investigated, mostly at relatively low pressures and temperatures.[20,21,29,33−43] In semicrystalline polymers, solubility of CO_2 occurs solely in amorphous regions. Plasticization of strained amorphous regions, such as those adjacent to crystalline lamella, may result in CO_2-induced crystallinity or "antiplasticization"[20,21] as found for poly(ethylene terephthalate) (PET)[34,36,37] and polycarbonate (PC).[35,44] Research on other semicrystalline polymers such as low-density polyethylene (LDPE),[38] poly(tetrafluoroethylene) (PTFE),[40] poly(vinylidene fluoride)[29] (PVDF) and polyurethanes[39] has been carried out at relatively low temperatures.

To evaluate supercritical CO_2 as a processing aid for semicrystalline polymers, information on plasticization approaching the melting temperature, T_m, is desirable. In addition, knowledge of the effect on T_m by CO_2 plasticization is required. T_m is defined as the temperature at which the chemical potentials of amorphous (μ_a) and crystalline phases (μ_{cry}) are equal. Thus, dissolution of CO_2 in the amorphous phase lowers μ_a and decreases T_m ($\Delta\mu_a = \Delta\mu_{cry}$).[45] For example, at 72 bar of CO_2 the T_m of syndiotactic PS (270 °C) is lowered by about 12 °C.[41]

Relatively little information exists on supercritical CO_2 plasticization effects on engineering thermoplastics at temperatures approaching T_m. In planning our work, we considered a number of methods, keeping in mind the demands of working at higher temperatures and pressures. On the basis of these requirements, an approach using a linear variable differential transformer (LVDT) was developed for direct measurement of polymer dilation.

In the LVDT method, the isolation of the magnet, which tracks sample dilation, from the external coil by an intervening nonmagnetic high-pressure steel pipe obviates the need for dynamic seals usually required for high-pressure work. Previously we reported LVDT measurement of polymer swelling for a styrene−butadiene−styrene triblock (SBS) elastomer and a polymer glass (PMMA).[46,47] We report below an investigation of polyvinylidene fluoride (PVDF), a semicrystalline fluoropolymer polymer which extends the LVDT application to higher temperatures and pressures. Constant tem-

10.1021/ma025929d CCC: $25.00
Published on Web 04/11/2003

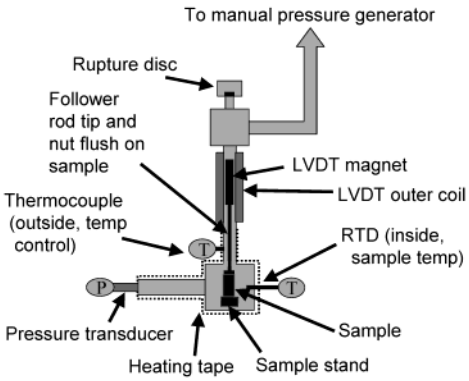

Figure 1. Illustration of the sample chamber section of the LVDT apparatus.

perature and constant pressure experiments are described that reveal differing aspects of supercritical CO_2 plasticization effects.

Experimental Section

1. Materials. Liquid CO_2 (99.8%) was obtained from Roberts Gas Co. Poly(vinylidene fluoride) (PVDF) homopolymer powder, Scientific Polymer Catalog no. 102, $M_w = 530\,000$ and $T_m = 158$ °C, was used as received. Circular PVDF disks were obtained by melt pressing the as received powder in a Carver Laboratory Press at 230 °C for 20 min. The melt pressed disk was rapidly cooled to room temperature by removing it from the press at 230 °C and air-cooling. For swelling measurements, rectangular bars (≈1 cm × 0.35 cm × 0.2 cm) were cut from melt pressed disks with a small saw. If needed, the sample was carefully sanded to regular dimensions after cutting. The mass of a typical sample was about 0.14 g.

2. Equipment. Differential scanning calorimetry (DSC) measurements were carried out using a Perkin-Elmer DSC Pyris-1.

(a) LVDT System. All pipes and fittings were stainless steel parts (316SS, pressure rating 1360 bar) obtained from High-Pressure Co. (HiP), Erie, PA. A Loctite Silver Grade antiseize joint lubricant obtained from McMaster-Carr was applied to chamber fittings to extend coupling life. Polymer swelling measurements in supercritical CO_2 were carried out in an apparatus consisting of a pressure generating section and a sample chamber (Figure 1). The pressure generating section (not shown) is similar to that employed previously for measuring polymer phase behavior in supercritical fluids.[48]

A standard LF9 T-fitting was employed as the sample chamber. A pressure transducer (Omega PX-602) rated at ±0.4% full scale (±3 bar) and resistive temperature device (RTD) were attached to the arms of the T. The vertical T-opening was attached to a nonmagnetic steel pressure pipe that was surrounded by the LVDT outer coil. The entire assembly was connected to the pressure generating section through an LF6 T-fitting.

Polymer swelling was measured with a LVDT coil (Schaevitz Sensors, Hampton, VA). The coil surrounded a section of the nonmagnetic steel pressure pipe described above. A thin (1.8 mm) nonmagnetic threaded follower rod (Schaevitz catalog no. 05282945-006) was fitted with a cylindrical magnet (2.8 mm OD, Schaevitz catalog no. 05561781-000) and placed inside the steel pressure pipe.

(b) Safety Features. A rupture disk (850 bar) was connected to the top of the T-fitting as shown in Figure 1. In addition to the measurement of pressure near the sample on the CO_2 side, a gauge was used to measure pressure on the water side (Standard Gauge 6PG20, HiP). The lowest pressure rated component in the system was rated to 1020 bar giving a substantial safety margin. A well secured, $^1/_4$ in. thick polycarbonate shield was placed between personnel and the high-pressure system. The pressure, temperature, and displacement meters were placed on the personnel side of the system.

3. Measurements. (a) Calibration. To calibrate the LVDT, the nonmagnetic follower rod was placed on the central shaft of an accurate dial micrometer. Changes in LVDT readings were noted as the micrometer shaft was moved in small increments. These data were used to obtain a calibration curve of LVDT voltage vs displacement of the follower rod.

(b) Linear Swelling. The sample bar was placed in the chamber on an insulated stage consisting of a thin graphite rod wrapped in aluminum foil. A small nut was fitted on the follower rod to distribute the mass of the magnet and follower rod (3 g) over the sample. The follower rod was then placed on the sample. Applying appropriate torque to the fitting connecting the sample chamber to the steel pressure pipe/LVDT assembly sealed the system. The sample chamber was purged with N_2 and heated to the desired temperature before introducing CO_2.

The sample size (≈0.07 cm^3, 0.14 g) resulted in a convenient rate of dilation for manual data collection. Typically, total time for data acquisition after a change in P or T was 2 h. The swelling results are reported as % change in the sample length $(\Delta L/L_o)$%, where $\Delta L = L_t - L_o$, L_t is the length of the sample at time t, and L_o is the original sample length. Data were not curve-fit; curves in figures are guides for the eye.

For constant temperature experiments, the sample was first heated to the desired temperature. Then, CO_2 was slowly introduced into the chamber and the pressure was increased to the first pressure stage, 138 bar. LVDT readings were noted at regular intervals. When the sample had attained maximum swelling, LVDT readings remained constant for 20−30 min. The pressure was then increased slowly to the next stage (276 bar) with the manual pressure generator and LVDT readings noted again. LVDT data was obtained from 138 to 670 bar. The same methodology was followed as the pressure was decreased from 670 to 138 bar. This allowed measurement and evaluation of hysteresis.

For constant pressure experiments, CO_2 pressure was increased to the desired value at a temperature below T_m. LVDT readings were noted at regular intervals. When the sample attained maximum swelling, the LVDT readings remained constant for 20−30 min. The temperature was then increased by 2−3 °C incrementally, while employing the manual pressure generator to maintain constant CO_2 pressure. At T_m, $\Delta L/L_o$ decreased markedly due to sample melting. The experiment was terminated a few degrees above T_m.

Results and Discussion

To expand studies evaluating plasticization and T_m depression of high temperature thermoplastics, we have developed a method that utilizes a linear variable differential transformer (LVDT). Our work has been initiated with polyvinylidene fluoride. The DSC of melt-pressed PVDF is shown in Figure 2. In addition to the large endothermic peak at ≈158 °C, there is a broad endotherm at 130−140 °C resulting from processing, since it is not seen in the second DSC scan. The lower melting point of this particular PVDF grade may reflect a relatively high head to head defect content.

LVDT Measurements. The sample chamber section of the LVDT apparatus for measuring linear swelling is shown in Figure 1. The design avoids custom machining and utilizes standard stainless steel parts. Sample preparation and loading is described in the Experimental Section.

Constant Temperature Experiments. Linear swelling in supercritical CO_2 was measured as a function of pressure at four temperatures. Figure 3 shows a representative plot of percent dilation $(\Delta L/L_o)$ as a function of time at 117 °C from 138 to 670 bar. Dilation increased with time and reached a maximum value at each

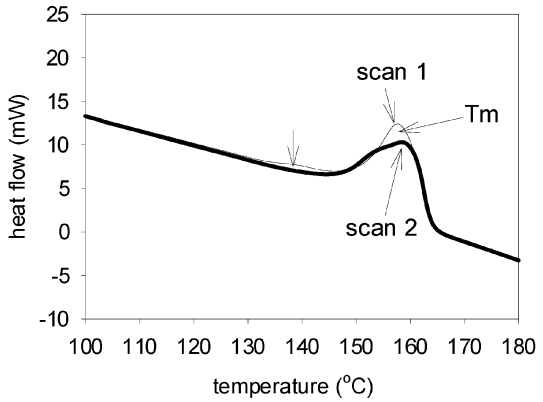

Figure 2. DSC scans for melt-pressed PVDF; heating rate is 10 °C/min.

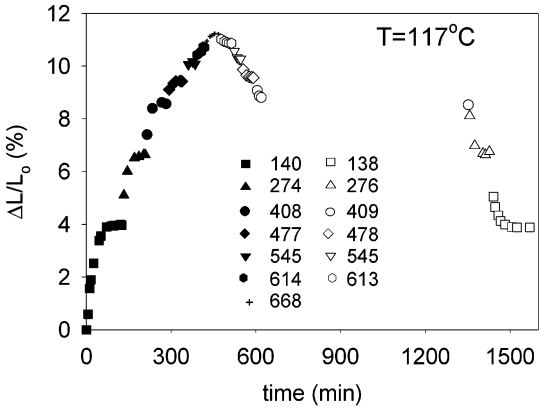

Figure 3. Percent dilation ($\Delta L/L_o$) as a function of time for PVDF in supercritical CO_2 at 117 °C. Filled symbols are for increasing pressure from 140 to 668 bar. Unfilled symbols are for pressure decreasing from 668 to 138 bar.

pressure. As CO_2 pressure was increased from 138 to 670 bar, $\Delta L/L_o$ increased from 4% to 12%.

Figure 3 also shows $\Delta L/L_o$ as pressure was decreased from 670 to 138 bar. By comparing the initial and final dilation measurements at 138 bar, hysteresis at 117 °C was determined to be negligible (0.1%). As a measure of system stability and evidence of equilibrium, as the pressure was decreased from 477 to 409 bar, $\Delta L/L_o$ decreased from 9.3% to 8.5% in 30 min and then remained constant for almost 800 min.

Swelling data for three additional temperatures was obtained in a similar fashion. Figure 4 shows a plot of $\Delta L/L_o$ as a function of pressure for four temperatures (75, 99, 117, and 130 °C). A strong dependence of swelling on CO_2 pressure and temperature is seen. In the vicinity of 75 °C, the shape of the swelling curve, is similar to that obtained using the ultrasonic/mercury method.[29] However, the LVDT data show higher dilation (3.9%, 75 °C, 276 bar) than that reported previously (1.2%, 80 °C, 300 bar). This may be a result of lower crystallinity in our PVDF samples. Alternatively, the container of mercury used in prior work may have constrained the sample and yielded a lower apparent dilation. We have noticed the effect of constraint on swelling when samples have been too large to swell freely. To avoid constraint and to ensure accurate temperature control, care must be taken to allow enough room for sample expansion and to prevent the sample from contacting the sample chamber walls. McCarthy has previously noted a constraint effect in that foaming

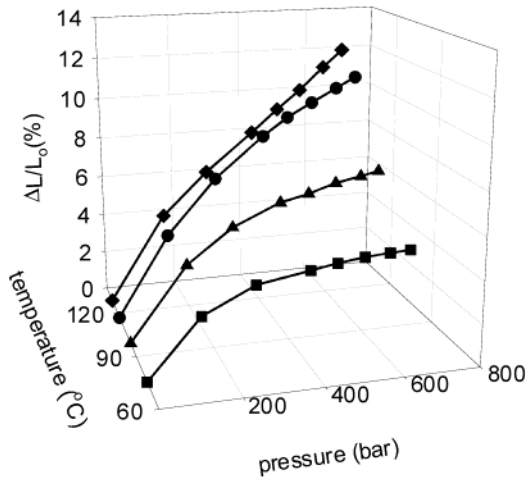

Figure 4. Percent dilation ($\Delta L/L_o$) as a function of pressure for PVDF in supercritical CO_2 at four temperatures: 75 °C (■), 99 °C (▲), 117 °C (●), and 130 °C (◆).

of PS is prevented in composites where PFA serves as the rigid matrix.[19]

At lower temperatures (75 and 99 °C), Figure 4 shows that $\Delta L/L_o$ attenuates above 414 bar. For example, at 75 °C, PVDF attains a maximum linear swelling of 4% from 276 to 414 bar. A subsequent increase in P from 414 to 670 bar results in a differential swelling ($d(\Delta L/L_o)/dP$) of only 1% [5% (at 676 bar) − 4% (at 414 bar)]. At 99 °C, $\Delta L/L_o$ is 6% at 414 bar. A differential swelling of only 1.5% is observed when the pressure is increased from 414 to 670 bar. Thus, rate of change of swelling with pressure, $d(\Delta L/L_o)/dP$, decreases dramatically at high CO_2 pressures.

This swelling behavior for PVDF at low temperatures shown in Figure 4 is similar to that observed for glassy polymers such as PMMA[23,31,49] and PS.[23,31] This observation is interesting given that the temperatures for PVDF swelling are well above T_g (−38 °C). For semicrystalline PVDF, the crystalline phase acts as junction points that restrict swelling. The swelling of semicrystalline polymers can be expressed as a sum of the mixing and elastic contributions based on the analogy of cross-linked network swelling.[45] Thus, the free energy change can be written as

$$\Delta G_{swell} = \Delta G_{mixing} + \Delta G_{elastic} \quad (1)$$

The polymer−solvent (PVDF−CO_2) interactions are included in the mixing contribution (ΔG_{mixing}). Swelling increases with the number and strength of the polymer−solvent interactions in comparison to polymer−polymer and solvent−solvent interactions. The elastic contribution ($\Delta G_{elastic}$) incorporates the constraining effect of the crystalline junction points and resistance to swelling which is a function of polymer modulus. Increasing number of junction points (or cross-links) decreases swelling. It is evident, then, that polymers with lower modulus should swell more due to a lower unfavorable elastic contribution. Thus, polymer swelling is a balance between the favorable mixing and unfavorable elastic contributions.

In Figure 5, $\Delta L/L_o$ and CO_2 density, respectively, are plotted as a function of pressure at 75 °C. The shape of the two curves is almost identical. Hence, for pressures below 414 bar, the rate of change of solvent quality (density) of supercritical CO_2 plays the most important

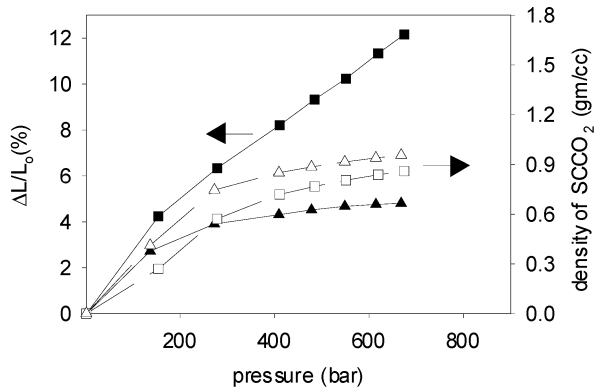

Figure 5. $\Delta L/L_o$ (%) (filled symbols) and CO_2 density (unfilled symbols) as a function of pressure at 130 (■, □) and 75 °C (▲, △), respectively.

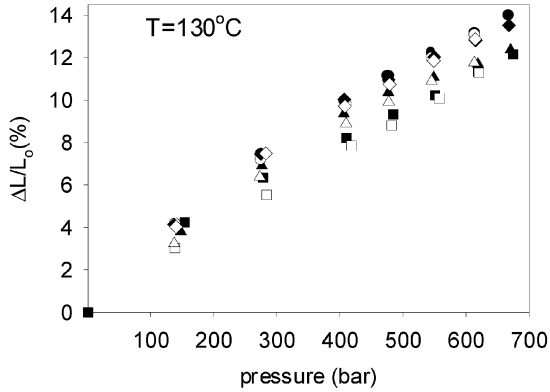

Figure 6. $\Delta L/L_o$ as a function of pressure for multiple cycles at 130 °C: increasing pressure, filled symbols; decreasing pressure, open symbols. Key: sample 1, run 1 (■, □); sample 2, run 1 (▲, △), run 2 (●, ○), and run 3 (◆, ◇).

role in determining extent of swelling. Increased CO_2 pressure augments the number of PVDF−CO_2 donor−(F−) acceptor (CO_2) interactions and increases swelling. This results in a significant increase in polymer plasticization with a small increase in pressure.

At pressures higher than 414 bar, hydrostatic pressure produces a "squeezing effect" leading to attenuated swelling.[22] As a result, the differential increase in differential swelling is much lower at pressures above 414 bar (Figure 4). Another reason for limited swelling above 414 bar is restriction of chain expansion due to "hardened" crystalline junction points and increased Young's modulus ($\sim 9.5 \times 10^3$ MPa at 80 °C).[50] Thus, by eq 1, the elastic contribution is negligible or even unfavorable depending on CO_2 pressure.

In contrast to the behavior below 100 °C, at higher temperatures (117 °C, 130 °C) increased swelling is strongly dependent on pressure up to 670 bar. For example at 117 °C, $\Delta L/L_o$ is 4% at 138 bar and 8% at 414 bar, giving a differential swelling of 4% corresponding to a 276 bar increase in pressure. On increasing pressure from 414 to 690 bar, $\Delta L/L_o$ increases to 12%, again giving a differential swelling of 4% for a 256 bar pressure increase. Figure 5 shows a plot of $\Delta L/L_o$ and the CO_2 density, respectively, as a function of pressure at 130 °C. The shapes of density and $\Delta L/L_o$ curves are not correlated at 130 °C. This is in contrast to resemblance of the density and dilation curves at 75 °C.

The different swelling behavior above and below about 100 °C is an interesting result stemming from the accuracy of the LVDT technique and the ability to work at high temperatures and pressures. An overall decreased resistance to swelling with increasing temperature is expected due decreased Young's modulus which, at ambient pressure, decreases from $\sim 9.5 \times 10^3$ MPa at 80 °C to $\sim 5 \times 10^2$ MPa at 120 °C.[50]

The DSC scan of melt-pressed PVDF (Figure 2) shows a broad endotherm between 130 and 140 °C, indicating presence of imperfect crystallites due to processing history. Lower melting crystals would experience a depression of T_m similar to that for the higher melting phase discussed below. Interestingly, the values of $d(\Delta L/L_o)/dP$ at the higher temperatures (117 and 130 °C), are almost identical ($\approx 6.8 \times 10^{-4}$ psi^{-1}). This implies that a majority of the imperfect crystallites melt at a temperature ≤117 °C. The greater dependence of swelling above 100 °C is therefore attributed to supercritical CO_2 induced melting of imperfect crystalline lamellae and the increasingly larger volume fraction of the amorphous phase. Apparently, this melting behavior weakens the network structure so that the amorphous phase is less constrained by physical cross-linking. The decrease in modulus together with reduction in constraint by junction points due to supercritical CO_2 induced melting of imperfect crystals results in a lower unfavorable elastic contribution in eq 1 and larger dilation.

Multiple Cycles: Hysteresis and Reproducibility. To explore accuracy and reproducibility, Figure 6 shows data at 130 °C for different samples and for multiple runs on the same sample. For two different samples, dilation was within 0.2% at low and high pressures, but a 1% divergence (higher for sample 2) occurred at intermediate pressures. Both samples exhibit slight hysteresis. For example, on increasing the pressure to 138 bar, linear swelling is 4% for sample 2. On returning to 138 bar after having increased pressure to 676 bar, a swelling of 3% is obtained giving a hysteresis of 1%.

Three runs were carried out on sample 2 at 130 °C. The maximum $\Delta L/L_o$ for sample 2 was 12% for run 1 and 14% for run 2. Run 3 gave virtually the same data as run 2 for increasing and decreasing pressure. In fact, it is difficult to follow the points for run 2 (●, ○) and run 3 (♦, ◇) as these points are often superimposed. The increased swelling for run 2 compared to run 1 is similar to "CO_2 conditioning" observed for glassy polymers in supercritical CO_2.[30,51] CO_2 conditioning has been attributed to structural relaxation of the glassy polymer chains. For the PVDF samples, we believe that residual strain is incorporated during sample preparation, and that relaxation occurs during the first run. This hypothesis is consistent with the reproducibility of PVDF swelling in supercritical CO_2 for runs 2 and 3. Thus, at 130 °C, the maximum swelling of PVDF is 14% at 676 bar.

Constant Pressure Experiments. The effect of temperature on swelling was investigated at constant pressure from 272 to 670 bar. Linear dilation ($\Delta L/L_o$) was measured at selected temperatures below T_m (158 °C). Once swelling reached a constant value, the temperature was increased by 2−3 °C and the measurement process was repeated.

Figure 7 shows a representative plot of $\Delta L/L_o$ as a function of time at 544 bar. Dilation increases with each increase of temperature, reaching a maximum in about 1 h. As the temperature increases from 130.6 to 137.8 °C, $\Delta L/L_o$ increases to 14%. However, at the next higher temperature (140.7 °C), $\Delta L/L_o$ decreases. Further increase to 142.3 °C results in a large decrease in $\Delta L/L_o$.

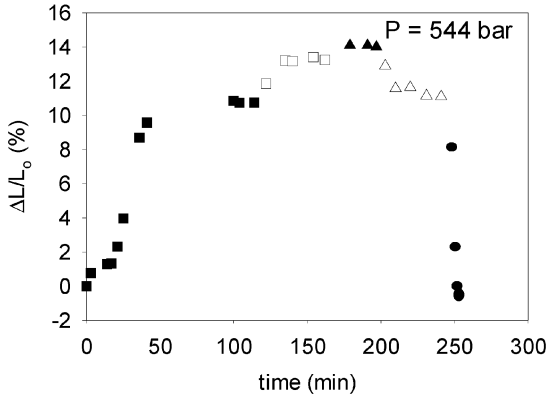

Figure 7. PVDF dilation as a function of time in CO_2 at 554 bar: Symbols represent temperatures from 130.6 to 142.3 °C: (■) 130.6 °C; (□) 134.7 °C; (▲) 137.8 °C; (△) 140.7 °C; (●) 142.3 °C.

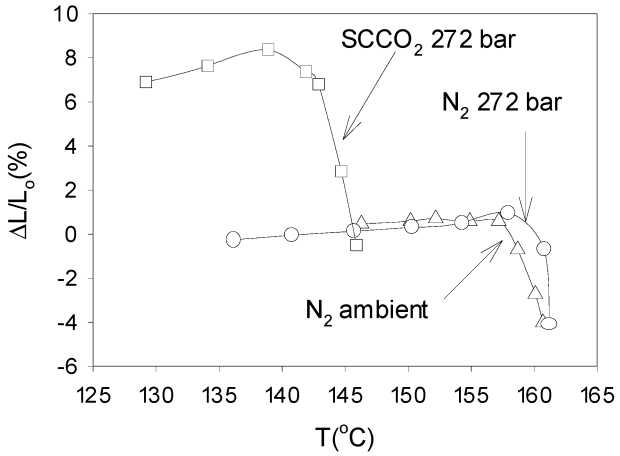

Figure 8. $\Delta L/L_o$ of PVDF as a function of temperature in various environments: (△) N_2 at ambient pressure; (○) N_2 at 272 bar; (□) CO_2 at 272 bar.

Figure 8 provides dilation data (T = 135−165 °C) in N_2 at ambient pressure and at 272 bar. At ambient pressure (T = 145−165 °C), $\Delta L/L_o$ is minimal reaching a maximum value of 0.1% before decreasing sharply between 157 and 159 °C. Because of the limited number of data points, T_m is designated as the temperature halfway between the temperature of maximum swelling and the temperature corresponding to loss of linear dimension. When this convention is chosen, temperatures near the maximum in the DSC endotherm (Figure 2) are obtained. Alternatively, the LVDT determined melting temperature may be described as the temperature at which $d(\Delta L/L_o)/dT$ becomes negative.

For N_2 at 272 bar, a small dilation is observed, reaching a maximum value of 1.8% (Figure 8). A decrease in $\Delta L/L_o$ indicates T_m at 159.4 °C, that is, an increase in T_m with increasing pressure. Figure 8 also shows dilation in supercritical CO_2 at 272 bar from 130 to 150 °C. In supercritical CO_2, $\Delta L/L_o$ reaches a maximum value of 11%. This is in marked contrast to the minimal swelling in N_2. The rapid decrease in $\Delta L/L_o$ at 140 °C corresponds to T_m, a decrease of about 18 °C compared to ambient pressure.

Figure 9 shows a plot of the T_m as a function of CO_2 pressure. As pressure is increased, T_m decreases to a minimum of 135 °C at 483 bar. The maximum T_m depression is 23 °C. Above 483 bar, T_m increases slowly to 137 °C at 670 bar, the experimental limit. As previously noted, this behavior is due to the opposing

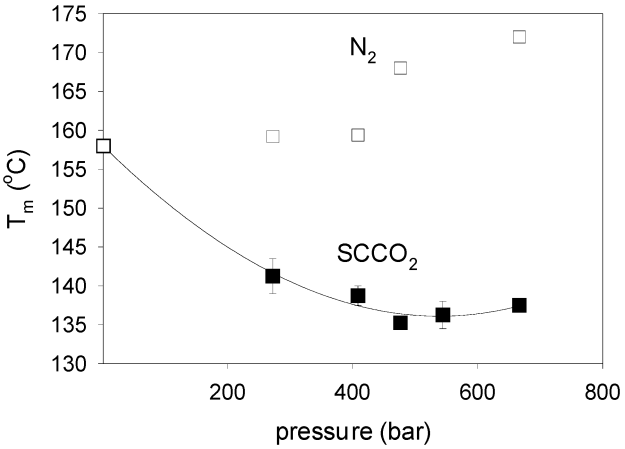

Figure 9. PVDF T_m as a function of pressure in CO_2 (■) and N_2 (□).

effects of increasing plasticization and higher hydrostatic pressure. At pressures below 483 bar, CO_2 plasticization lowers T_m. Above 483 bar, hydrostatic pressure effects overcome plasticization and T_m increases, albeit slowly. Previous work utilizing hydrostatic pressure alone showed T_m increases ≈1 °C/31 bar.[52,53]

The contrasting effects of N_2 pressure on PVDF T_m are seen in Figure 9. Plasticization by N_2 is considerably smaller than for CO_2 (1.8% vs 11%, respectively, at 272 bar and 145 °C). Hence the increased T_m reflects primarily the effect of nitrogen hydrostatic pressure. As pressure is increased to 272 bar, there is a small increase in T_m to 159.4 °C (ΔT_m, 1.4 °C). Increasing the pressure to 408 bar does not significantly alter the T_m. However, on an increase of pressure to 483 bar, T_m increases to 168 °C. Further increases in pressure cause increases in T_m to 172 °C at 680 bar. For N_2, a "noninteracting gas" [54] melting point depression is not observed despite slight plasticization. Rather, hydrostatic pressure effects dominate and result in increasingly higher melting temperatures with increases in pressure.

An interesting feature seen in Figure 9 is the nonlinearity in the relationship of T_m to nitrogen pressure. Between 400 and 500 bar there is a jump of 10 °C in T_m. Evidently, hydrostatic pressure effects are especially effective in this pressure range, resulting in an increase in PVDF T_m. Interestingly the maximum lowering of PVDF T_m (23 °C) in supercritical CO_2 occurs in this pressure range. Thus, this pressure (400−500 bar) corresponds to the leveling off of the effect of CO_2 plasticization vs hydrostatic pressure effects. Currently we are evaluating the morphology of post-plasticized PVDF by a number of techniques to help elucidate this phenomenon.

Conclusions

The plasticization of PVDF by supercritical CO_2 was investigated by employing an LVDT-based system. This technique measures change in length or swelling of the polymer sample in one dimension with minimal data processing. Additionally, this technique isolates the measurement device from supercritical CO_2. The presence of dynamic seals is avoided, and high pressures and temperatures are readily employed.

In constant temperature experiments (75, 99, 117, and 130 °C), CO_2 pressure was increased from 138 to 670 bar. At 75 and 99 °C, the CO_2 density or solvent quality determines the extent of swelling. At lower

pressures, the rate of change of dilation with pressure ($d(\Delta L/L_o)/dP$) increases rapidly as a function of pressure up to 414 bar and then attenuates. At higher temperatures (117 and 130 °C), $d(\Delta L/L_o)/dP$ is almost linear. The higher swelling of PVDF above 100 °C is attributed to an overall decrease in modulus with increasing temperature together with decreased constraint of the amorphous phase by junction points due to CO_2 induced melting of imperfect crystals.

In constant pressure experiments (138−670 bar), PVDF swelling was measured as a function of temperature. As a baseline for constant pressure experiments, LVDT and DSC data in nitrogen at 1 bar were compared. We define T_m as the midpoint between the temperature of maximum expansion and temperature of initial loss of linear dimension. Thus, at constant CO_2 pressure, T_m depression is readily determined by increasing temperature in small increments. As pressure increased, T_m decreased reaching a minimum of 135 °C at 483 bar. At higher pressures (≥544 bar), T_m increases as hydrostatic pressure effects become important. Unlike CO_2, PVDF plasticization by N_2 is minimal. T_m increases with increasing pressure, particularly at pressures ≥483 bar due to effect of hydrostatic pressure.

At the end of the constant pressure experiments, the recrystallization from the melt takes place in the presence of supercritical CO_2. At the end of constant temperature experiments the sample has been annealed in supercritical CO_2. In a future paper, we will report on the morphological consequences of these different processes.

Acknowledgment. The authors dedicate this paper to the memory of Mr. K. Ohsaka, formerly of Daikin Industries, Ltd., and to Dr. C. Stewart of the Daikin Institute for Advanced Chemistry and Technology (DAI-ACT), who were essential in initiating our supercritical CO_2 program. The authors also acknowledge Prof. Mark McHugh and Mr. Alberto Garach-Domech for their help. Financial support from DAI-ACT and from the VCU School of Engineering Foundation is gratefully acknowledged.

Note Added after ASAP Posting. This article was released ASAP on 04/11/2003 with errors in the caption to Figure 8. The caption has been changed for clarity and the correct version was posted on 04/21/2003.

References and Notes

(1) McHugh, M. A.; Krukonis, V. J. *Supercritical Fluid Extraction*; Butterworth-Heimann: Newton, MA, 1994.
(2) Kirby, C. F.; McHugh, M. A. *Chem. Rev.* **1999**, *99*, 565−602.
(3) Ajzenberg, N.; Trabelsi, F.; Recasens, F. *Chem. Eng. Technol.* **2000**, *23*, 829−839.
(4) Cooper, A. I. *J. Mater. Chem.* **2000**, *10*, 207.
(5) Canelas, D. A.; Burke, A. L. C.; DeSimone, J. M. *Plast. Eng.* **1997**, *53*, 37−40.
(6) Hoggan, E. N.; Kendall, J. L.; Flowers, D.; Carbonell, R. G.; DeSimone, J. M. *Abstr. Pap. Am. Chem. Soc.* **1999**, *218*, 52-PMSE.
(7) Arora, K. A.; Lesser, A. J.; McCarthy, T. J. *Macromolecules* **1998**, *31*, 4614−4620.
(8) Beaucage, G.; Aubert, J. H.; Lagasse, R. R.; Schaefer, D. W.; Rieker, T. P.; Erlich, P.; Stein, R. S.; Kulkarni, S.; Whaley, P. D. *J. Polym. Sci., Part B: Polym. Phys.* **1996**, *34*, 3063−3072.
(9) Goel, S. K.; Beckman, E. J. *Polym. Eng. Sci.* **1994**, *34*, 1137−1147.
(10) Handa, Y. P.; Zhang, Z. Y. *J. Polym. Sci., Part B: Polym. Phys.* **2000**, *38*, 716−725.
(11) Krause, B.; Mettinkhof, R.; van der Vegt, N. F. A.; Wessling, M. *Macromolecules* **2001**, *34*, 874−884.
(12) Utracki, L. A. S. R. *J. Polym. Sci., Part B: Polym. Phys.* **2001**, *39*, 342.
(13) Sun, H.; Mark, J. E. *J. Appl. Polym. Sci.* **2002**, *86*, 1692.
(14) Royer, J. R.; Gay, Y. J.; DeSimone, J. M.; Khan, S. A. *J. Polym. Sci., Part B: Polym. Phys.* **2000**, *38*, 3168−3180.
(15) Elkovitch, M. D.; Lee, L. J.; Tomasko, D. L. *Polym. Eng. Sci.* **2000**, *40*, 1850−1861.
(16) Conway, S. E.; Lim, J. S.; McHugh, M. A.; Wang, J. D.; Mandel, F. S. *J. Appl. Polym. Sci.* **2001**, *81*, 2642−2648.
(17) Kwag, C.; Manke, C. W.; Gulari, E. *Ind. Eng. Chem. Res.* **2001**, *40*, 3048−3052.
(18) Hobbs, T.; Lesser, A. J. *Polym. Eng. Sci.* **2001**, *41*, 135−144.
(19) Arora, K. A.; Lesser, A. J.; McCarthy, T. J. *Macromolecules* **1999**, *32*, 2562−2568.
(20) Handa, Y. P.; Roovers, J.; Wang, F. *Macromolecules* **1994**, *27*, 5511.
(21) Handa, Y. P.; Zhang, Z. Y.; Roovers, J. *J. Polym. Sci., Part B: Polym. Phys.* **2001**, *39*, 1505−1512.
(22) Wang, W. V.; Kramer, E.; Sachse, W. H. *J. Polym. Sci., Part B: Polym. Phys.* **1982**, *20*, 1371.
(23) *High-Pressure Solid Polymer-Supercritical Fluid Phase Behvaior*; Liau, I. S., McHugh, M. A., Eds.; Elsevier Science Publishers: Amsterdam, The Netherlands, 1985.
(24) Chiou, J. S.; Barlow, J. W.; Paul, D. R. *J. Appl. Polym. Sci.* **1985**, *30*, 2633.
(25) Wissinger, R. G.; Paulaitis, M. E. *J. Polym. Sci., Part B: Polym. Phys.* **1987**, *25*, 2497.
(26) Condo, P. D. J.; K. P. *J. Polym. Sci., Part B: Polym. Phys.* **1994**, *32*, 523.
(27) Kamiya, Y. M.; Keishin; Terada, Katsuhiko; Fujiwara, Yukihiko; Wang, Jin-Sheng. *Macromolecules* **1998**, *31*, 472.
(28) Royer, J. R.; DeSimone, J. M.; Khan, S. A. *Macromolecules* **1999**, *32*, 8965−8973.
(29) Briscoe, B. J.; Lorge, O.; Wajs, A.; Dang, P. *J. Polym. Sci., Part B: Polym. Phys.* **1998**, *36*, 2435.
(30) Wang, J. S.; Kamiya, Y.; Naito, Y. *J. Polym. Sci., Part B: Polym. Phys.* **1998**, *36*, 1695−1702.
(31) Zhang, Y. G.; K. K.; Lemert, R. M. *J. Supercrit. Fluids* **1997**, *11*, 115.
(32) Handa, Y. P.; Kruus, P.; Oneill, M. *J. Polym. Sci., Part B: Polym. Phys.* **1996**, *34*, 2635−2639.
(33) Zhong, Z. K.; Zheng, S. X.; Mi, Y. L. *Polymer* **1999**, *40*, 3829−3834.
(34) Chiou, J. S.; Barlow, J. W.; Paul, D. R. *J. Appl. Polym. Sci.* **1985**, *30*, 3911.
(35) Gross, S. M. R.; G. W.; Kiserow, D. J.; DeSimone, J. M. *Macromolecules* **1999**, *32*, 8965.
(36) Koros, W. J. P.; D. R. *J. Polym. Sci.: Part B: Polym. Phys.* **1978**, *16*, 1947.
(37) Mizoguchi, K. H.; Takuji; Naito, Yasutoshi; Kamiya, Yoshinori. *Polymer* **1987**, *28*, 1298.
(38) Shieh, Y. T.; Su, J. H.; Manivannan, G.; Lee, P. H. C.; Sawan, S. P.; Spall, W. D. *J. Appl. Polym. Sci.* **1996**, *59*, 707−717.
(39) Briscoe, B. J.; Kelly, C. T. *Polymer* **1995**, *36*, 3099−3102.
(40) Briscoe, B. J.; Zakaria, S. *J. Polym. Sci., Part B: Polym. Phys.* **1991**, *29*, 989.
(41) Handa, Y. P.; Zhang, Z. Y.; Wong, B. *Macromolecules* **1997**, *30*, 8499−8504.
(42) Hatada, K.; Kitayama, T.; Ute, K.; Fujimoto, N.; Miyatake, N. *Macromol. Symp.* **1994**, *84*, 113−126.
(43) Singh, M. A.; Hutanu, R.; Shea, M.; Fraser, R.; Plivelic, T.; Handa, Y. P. *J. Polym. Sci., Part B: Polym. Phys.* **2000**, *38*, 2457−2467.
(44) Mi, Y. L.; Zheng, S. X. *Polymer* **1998**, *39*, 3709−3712.
(45) Flory, P. J. *Principles of Polymer Chemistry*; Cornell University Press: Ithaca, NY, 1953.
(46) Shenoy, S. L.; Sebra, B.; Woerdeman, D.; Garach, A.; McHugh, M.; Wynne, K. *Abstr. Pap. Am. Chem. Soc.* **2001**, *221*, 156-PMSE.
(47) Wynne, K. J.; Shenoy, S. L.; Fujiwara, T.; Irie, S.; Woerdeman, D.; Sebra, R.; Garach, A.; McHugh, M. A. *Abstr. Pap. Am. Chem. Soc.* **2002**, *224*, 660-POLY.
(48) Lora, M.; Lim, J. S.; McHugh, M. A. *J. Phys. Chem. B* **1999**, *103*, 2818−2822.
(49) Wissinger, R. G.; Paulaitis, M. E. *J. Polym. Sci., Part B: Polym. Phys.* **1991**, *29*, 631.
(50) Giannetti, E. *Polym. Int.* **2001**, *50*, 10.
(51) Tanaka, K.; Ito, M.; Kita, H.; Okamoto, K.; Ito, Y. *Bull. Chem. Soc. Jpn.* **1995**, *68*, 3011−3017.
(52) Hattori, T. H. M.; Hikosaka, M.; Ohigashi, H. *Polymer* **1996**, *37*, 85.
(53) Mekhilef, N. *J. Appl. Polym. Sci.* **2001**, *80*, 230−241.
(54) Mulder, M. *Basic Principles of Membrane Technology*; 2nd ed.; Kluwer Academic Publishers: Boston, MA, 1997.

MA025929D